

Dual-Polarization Radar Retrievals of Coastal Pacific Northwest Raindrop Size Distribution Parameters Using Random Forest Regression

ROBERT CONRICK, JOSEPH P. ZAGRODNIK, AND CLIFFORD F. MASS

Department of Atmospheric Sciences, University of Washington, Seattle, Washington

(Manuscript received 25 June 2019, in final form 31 October 2019)

ABSTRACT

Radar retrievals of drop size distribution (DSD) parameters are developed and evaluated over the mountainous Olympic Peninsula of Washington State. The observations used to develop retrievals were collected during the 2015/16 Olympic Mountain Experiment (OLYMPEX) and included the NASA S-band dual-polarimetric (NPOL) radar and a collection of second-generation Particle Size and Velocity (PARSIVEL²) disdrometers over the windward slopes of the barrier. Nonlinear and random forest regressions are applied to the PARSIVEL² data to develop retrievals for median volume diameter, liquid water content, and rain rate. Improvement in DSD retrieval accuracy, defined by the mean error of the retrieval relative to PARSIVEL² observations, was achieved when using the random forest model when compared with nonlinear regression. Evaluation of disdrometer observations and the retrievals from NPOL indicate that the radar retrievals can accurately reproduce observed DSDs in this region, including the common wintertime regime of small but numerous raindrops that is important there. NPOL retrievals during the OLYMPEX period are further evaluated using two-dimensional video disdrometers (2DVD) and vertically pointing Micro Rain Radars. Results indicate that radar retrievals using random forests may be skillful in capturing DSD characteristics in the lowest portions of the atmosphere.

1. Introduction

Precipitating weather events can be observed in three dimensions thanks to the continuous spatial and temporal coverage of meteorological ground-based radars, making radar observations a valuable tool for weather analysis and research. Radar products have long been used for microphysical retrievals, such as rain rate and drop size distribution (DSD) characteristics. Perhaps the first such retrieval was described in Marshall and Palmer (1948), who used reflectivity Z to estimate rain rate R at the surface using a power-law relation, known as a Z - R relationship. A number of such Z - R retrievals have since been developed for a variety of meteorological situations and locations, and they continue to be used by the U.S. National Weather Service to produce operational quantitative precipitation estimates (Kuligowski 1997; Fulton 2002; Apffel et al. 2015).

With the introduction of dual-polarization radars for research and operational applications (Kumjian 2013), microphysical retrievals of increased complexity have been developed from collocated radar and surface

observations, with substantial progress made during field experiments such as the NASA Global Precipitation Measurement (GPM) Mission Ground Validation (GV) campaigns. These campaigns include the deployment of sophisticated networks of remote and in situ observing platforms, coupled with data from the NASA GPM satellite (Hou et al. 2014). GPM GV projects such as the Midlatitude Continental Convective Clouds Experiment (MC3E; Jensen et al. 2016) and the Iowa Flood Studies (IFloodS; Krajewski et al. 2013) have provided valuable surface-based observations of precipitation and facilitated radar retrievals of microphysical properties (e.g., Pippitt et al. 2015). In addition to NASA GPM GV, a number of other studies have developed radar retrievals for DSDs using similar suites of observations (e.g., Brandes et al. 2006; Cao et al. 2008; Zhang et al. 2006). However, these experiments predominantly sampled convective environments in regions of relatively homogenous terrain and are not necessarily applicable to regions dominated by stratiform precipitation or regions with substantial topography.

Several studies have examined DSDs during stratiform or convective precipitation, delineating these regimes based on the DSD median volume diameter and

Corresponding author: Robert Conrick, rconrick@uw.edu

DOI: 10.1175/JTECH-D-19-0107.1

© 2020 American Meteorological Society. For information regarding reuse of this content and general copyright information, consult the [AMS Copyright Policy](#) (www.ametsoc.org/PUBSReuseLicenses).

the intercept parameter of the distribution (e.g., Tokay and Short 1996; Atlas et al. 1999; Bringi et al. 2003, 2009; Uijenoet et al. 2003; Siefert 2005; Sharma et al. 2009). Although Thompson et al. (2015) found considerable overlap of DSD characteristics between convective and stratiform environments, convection appeared to have larger liquid water content for a given drop size. Furthermore, Dolan et al. (2018) used principal component analysis to demonstrate that global DSD characteristics varied as a function of latitude, which, they suggested, meant that the physical processes impacting DSDs also varied by latitude.

The results of the above studies and others suggest that DSD radar retrieval algorithms developed for convective storms may not be applicable to locations where stratiform precipitation is dominant or where topography is a key controller of regional precipitation distributions, such as the Pacific Northwest (Chow et al. 2013). Zagrodnik et al. (2018), using DSD observations from the Olympic Mountains Experiment (OLYMPEX; Houze et al. 2017), showed that DSDs varied considerably during different storm sectors of midlatitude cyclones impacting the Olympic Peninsula of Washington State. In addition, they found that periods warm-rain enhancement were associated with DSDs having a large number of small drops.

The development of machine learning techniques and their implementations (e.g., the “scikit-learn” Python package; Pedregosa et al. 2011) provide new opportunities for the atmospheric sciences, particularly with regard to statistical weather forecasting (Herman and Schumacher 2018). To the best of our knowledge, however, there have been no applications of machine learning to DSD radar retrieval development, particularly in the Pacific Northwest. As such, this paper will apply a common machine learning algorithm [random forest (RF) regression; Breiman 2001] to disdrometer data to produce radar retrievals of DSD characteristics. One goal of this paper is to determine whether the random forest technique can be a feasible method to retrieve DSDs.

The central aim of this study is to produce and evaluate radar retrievals of median volume diameter, liquid water content, and rain rate over the Olympic Peninsula using OLYMPEX observations, specifically the NASA S-band dual-polarimetric (NPOL) radar and OLYMPEX disdrometers. This study develops and evaluates retrievals based on both traditional nonlinear regression and random forest regression techniques. Retrievals are then used to produce DSD information above the surface, where these observations are generally unavailable. Such radar-based retrievals could help evaluate microphysical biases in regional numerical weather prediction models, such as the documented underprediction of liquid water content and precipitation over windward slopes of the Pacific Northwest (Conrick and Mass 2019a,b). In

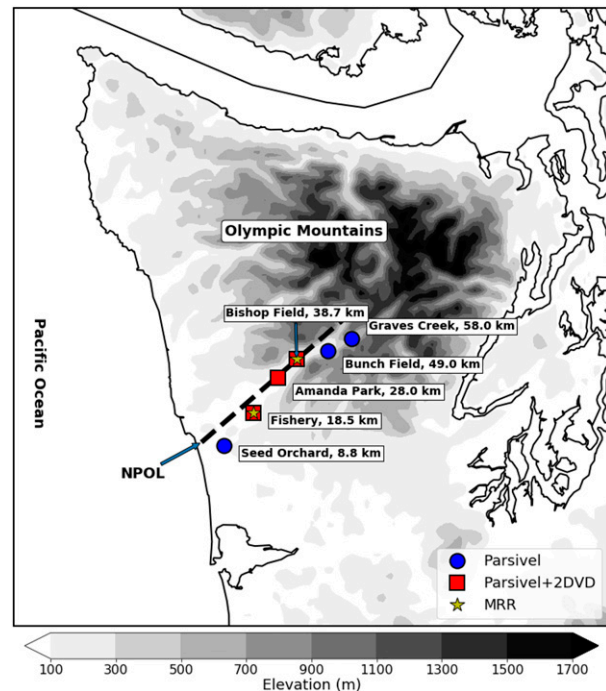


FIG. 1. Map of surface observing stations used in this study, including the NPOL radar, the PARSIVEL² units (blue circles), PARSIVEL² + 2DVD units (red squares), and MRR locations (stars). The black dashed line represents the 49.9° NPOL RHI scan that is used to develop retrievals. Distances from the NPOL radar to each station are also noted next to the station name.

this paper, section 2 describes the data and method used to retrieve microphysical information from radar data using second-generation Particle Size and Velocity (PARSIVEL²) disdrometer observations, and section 3 provides an evaluation of the retrievals using two-dimensional video disdrometers (2DVD) and vertically pointing radars. Section 4 includes discussion of results and concluding remarks.

2. Data acquisition and processing

a. NPOL radar data

During OLYMPEX, the NPOL (Wolff et al. 2017) radar provided coverage over the Quinalt Valley on the windward side of the Olympic Peninsula of Washington State (Fig. 1). The NPOL radar operated at a frequency of 2.77 GHz (108-mm wavelength). This study uses radar Z and differential reflectivity Z_{DR} over the Quinalt Valley collected along the 49.9° azimuth range–height indicator (RHI) scans with elevation angles ranging from 0° to 45°. Radar data were collected between 1 November 2015 and 1 February 2016. The NPOL range gate spacing during OLYMPEX was 125 m, and we remove data at the lowest elevation angle (0°). The temporal resolution of

the NPOL radar was approximately 20 min for the 49.9° RHI azimuth.

NPOL data underwent extensive quality control and data filtering following the conclusion of OLYMPEX (Wolff et al. 2017). The quality control process included the Global Precipitation Mission Ground Validation (GPM-GV) dual-polarimetric quality control (DPQC) algorithm (Pippitt et al. 2013). The DPQC algorithm is designed to filter raw radar data to remove erroneous data obtained by a radar system (e.g., ground clutter, biological targets, and anomalous propagation) by constraining measurements according to a number of numeric thresholds. Pippitt et al. (2013) describes the full process and physical basis for the algorithm.

Because the DPQC does not correct for signal attenuation, we apply the “ZPHI” attenuation correction method (Bringi et al. 1990; Gu et al. 2011; Ryzhkov et al. 2014) to the NPOL data. Despite S-band radars exhibiting less attenuation than do radars with smaller wavelengths (Bringi et al. 2012; Baldini et al. 2012), the presence of heavy rain near orography motivates the need to correct attenuation, as demonstrated by Ryzhkov et al. (2014), who showed that this technique is advantageous in regions of complex terrain. For this study, we use the ZPHI algorithm in the Python ARM Radar Toolkit (Py-ART) software—see Helmus and Collis (2016) for further details.

b. PARSIVEL² disdrometer and 2DVD

Along with the NPOL radar, several PARSIVEL² disdrometers (Petersen et al. 2017a) were positioned along a southwest-to-northeast line extending from the Pacific Coast to the Quinault Valley and adjacent windward slopes (Fig. 1). At each disdrometer site, liquid water content (LWC; g m^{-3}), median volume diameter D_0 (mm), rain rate (RR; mm h^{-1}), and the normalized DSD intercept parameter N_W ($\text{mm}^{-1} \text{m}^{-3}$; Illingworth and Blackman 2002) were calculated every minute from PARSIVEL² data using the PyDisdrometer software package (Hardin and Guy 2017), which uses Eq. (6) from Tokay et al. (2014) to compute DSDs.

At three PARSIVEL² locations (Fishery, Amanda Park, and Bishop Field) there were collocated 2DVDs (Petersen et al. 2017b). DSD information was computed in the same manner as the PARSIVEL² disdrometers and subject to the same quality control described below. The 2DVDs serve as an independent evaluation of this study’s DSD retrievals.

c. Data alignment and quality control

Initial quality control and data filtering of the PARSIVEL² and 2DVD datasets was completed as per NASA’s data management protocol, which removes

spurious drops from the disdrometer dataset. The protocol follows Tokay et al. (2001), in which drops are removed from the dataset if their fall velocity is $\pm 50\%$ of the empirical value from Beard (1976) for an identical sized drop. This ensures that erroneous data, which often appear as drops with unphysical fall speeds, are removed.

To facilitate the evaluation of radar retrieval products, NPOL data must be spatially and temporally aligned with ground assets (PARSIVEL² and 2DVD). Spatial alignment was performed by finding the horizontal location of each surface station in the 49.9° RHI, then obtaining the mean value of NPOL data (Z or Z_{DR}) within a ± 5 horizontal and ± 1 vertical range located around each surface site. These steps reduced inclusion of erroneous radar data (e.g., ground clutter) into the retrieval evaluations. For the Seed Orchard, Fishery, Amanda Park, Bishop Field, Bunch Field, and Graves Creek sites, the lowest NPOL gate used in evaluations corresponds to an approximate height of 133, 236, 314, 425, 1010, 1375 m above ground level (AGL), respectively, in order of distance from NPOL.

Next, data were matched in time. Surface station data were matched to NPOL observation times to the nearest minute, producing 2520 potential samples of data per station for subsequent evaluation. Next, data from all three surface-based platforms [PARSIVEL², 2DVD, and Micro Rain Radar (MRR)] were removed when any of the following conditions were met: 1) data were missing, null, or showed an error code; 2) $Z > 50 \text{ dBZ}$; 3) $Z_{\text{DR}} < -5 \text{ dB}$ or $Z_{\text{DR}} > 5 \text{ dB}$; 4) PARSIVEL² RR was less than 0.254 mm h^{-1} (this value corresponds to 0.01 in. h^{-1} , which is one tip of a standard tipping-bucket rain gauge); or 5) PARSIVEL² LWC was less than 0.01 g m^{-3} . NPOL data were removed from consideration if RR was less than 0.01 mm h^{-1} . The quality control steps above ensured that only precipitating times were considered.

d. Micro Rain Radar data

Evaluating radar retrievals above the surface presents a significant challenge due to a lack of microphysical observations. During OLYMPEX, two MRRs (Petersen and Gatlin 2017) from METEK were deployed at the Fishery and Bishop Field sites along the transect in Fig. 1. The MRR is a single-polarized, vertically pointing, 24-GHz (K band) radar that sampled 30 range gates from 0 to 3 km above ground at 100-m intervals. The MRR retrieves reflectivity and particle fall speed spectra, which are then converted into bulk radar reflectivity and DSDs with the Atlas et al. (1973) fall speed–drop size relation. Peters et al. (2005) provides a detailed description of the default MRR data processing and computations. From the MRRs, we computed 1-min values of Z , D_0 , LWC, N_W , and RR with the same method used to

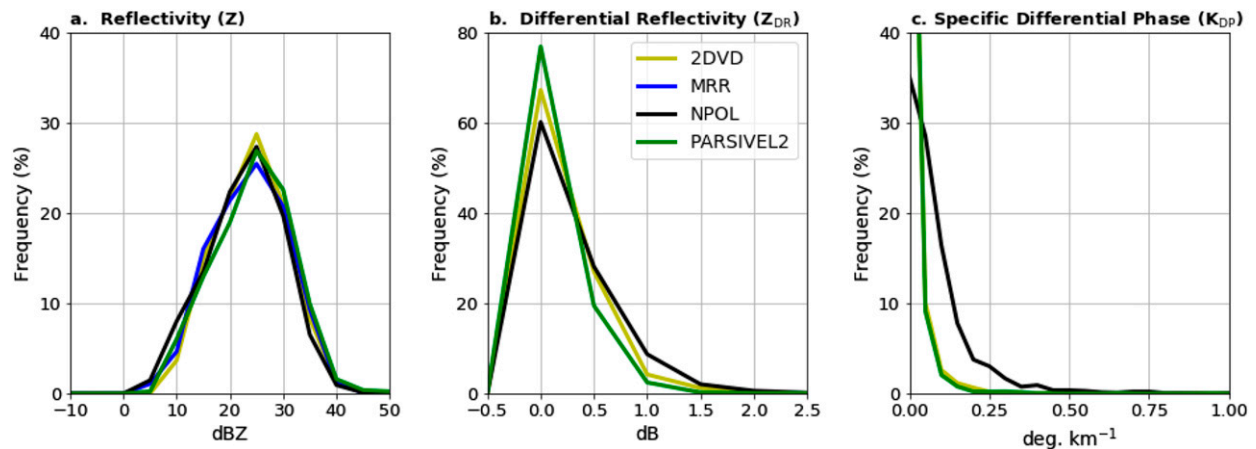


FIG. 2. Frequency distributions of (a) reflectivity Z , (b) differential reflectivity Z_{DR} , and (c) specific differential phase K_{DP} as observed by the NPOL radar and from T-matrix calculations applied to disdrometer (PARSIVEL² and 2DVD) and MRR observations. Colored lines represent the various datasets evaluated in this study. NPOL reflectivity and differential reflectivity data are bias corrected using the ZPHI method. No MRR data are shown in (b) or (c) because the MRR is a single-polarized instrument.

process the disdrometer data. MRR reflectivity data were computed by integrating the measured drop size distribution, rather than using a reflectivity factor computed from radar properties and particle cross-sectional areas.

Because the MRR operates at a wavelength that is approximately one tenth of the NPOL radar wavelength, attenuation due to liquid water is potentially significant and increases with height (METEK 2009; Peters et al. 2005), leading to reduced accuracy above the surface. To address attenuation concerns, MRR observations are bias corrected using the method described in the METEK Physical Basics document (METEK 2009). In short, their method of attenuation correction uses the path-integrated attenuation (PIA) calculated at each range gate to adjust the reflectivity spectrum retrieved at that particular range gate. The correction is only applied when PIA is less than 10 dB. In this study, we only consider attenuation-corrected MRR observations. Additionally, because stratiform precipitation tends to dominate wintertime conditions in the region of interest, we did not implement vertical velocity corrections to the MRR data as in Adirosi et al. (2016).

3. Retrieval methods

a. DSD radar scattering properties from PARSIVEL²

A goal of developing radar retrieval equations is to obtain information about the characteristics of DSDs (D_0 , LWC, RR, and N_w) over a wide area above the surface by using only ground-based observations. During OLYMPEX, PARSIVEL² disdrometers provided the greatest spatial and temporal coverage compared to

2DVD or MRR assets. As such, the T-matrix scattering method (Mishchenko et al. 1996) is applied to PARSIVEL² DSDs to estimate Z and Z_{DR} . These scattering calculations were performed using the NPOL radar frequency (2.77 GHz) and the Thurai and Bringi (2005) drop shape model within the framework of the PyDSD (Hardin and Guy 2017) software package.

Using Z and Z_{DR} estimated from T-matrix calculations, rather than directly from NPOL observations, is advantageous for producing accurate radar retrievals. Retrieval development using Z and Z_{DR} from NPOL produces significantly less accurate retrievals than the T-matrix method, likely because NPOL observations contain attenuation or ground clutter errors. Furthermore, the difference in height between the radar's lowest sample volumes and the surface increases with distance from the radar, which introduces additional uncertainty in the resulting retrieval. Thus, the T-matrix computation provides a more reliable conversion between radar scattering characteristics and DSD properties.

Figure 2 demonstrates the agreement between observed (NPOL) and disdrometer-derived radar parameters aggregated across all surface observing stations deployed during OLYMPEX. For these surface measurements, agreement is qualitatively good among all data sources, with no significant discrepancies between platforms. Comparing NPOL observations with the other platforms, Z from NPOL is slightly smaller (~ 3 dB) than the disdrometers (Fig. 2a), even though attenuation correction is applied to NPOL. Similarly, Z_{DR} is modestly larger from NPOL than the other observations (Fig. 2b), but mostly at large Z_{DR} . We suspect that these differences may be a result of the NPOL beam height being

well above the surface at the corresponding stations. Quantitatively, it is noteworthy that no dataset differs from one another in a statistically significant manner based on a Kolmogorov–Smirnov test of distribution similarity. Also, despite the relationship between specific differential phase K_{DP} and rain intensity demonstrated by Chandrasekar et al. (2008), K_{DP} is not used to develop retrievals because of the significant discrepancies between NPOL and PARSIVEL² K_{DP} values (Fig. 2c).

b. Nonlinear and random forest regression techniques

Prior to developing retrievals from random forests, it is important to produce a set of retrievals from nonlinear regression (NL), which is presently the most widely accepted method for generating radar retrievals. The retrievals shown in Table 1 were derived using least squares NL regression between PARSIVEL² observations and radar scattering properties from the T-matrix calculations. This method has been employed successfully by a number of other studies for a variety of environments and precipitation regimes (e.g., Zhang et al. 2001; Bringi et al. 2003; Brandes et al. 2004a,b; Cao et al. 2008; Gorgucci et al. 2008; Thurai et al. 2010; Pippitt et al. 2015). Following Carlin et al. (2016), our retrievals take the form of the product of power-law functions involving radar properties (Z and Z_{DR}) as independent variables.

Next, a second set of NPOL radar retrievals was developed using RF regression. RFs are an ensemble of decision trees that produce a single output value derived from a set of input data. Each tree is a network of connected decision nodes that terminate in leaf nodes. Beginning with an input value at the root (top) of a decision tree, the input traverses the tree toward subsequent nodes along a left or right branch based on a numerical assessment at each decision node. When the input value reaches a leaf node (the bottom of the tree), then the decision tree has been fully traversed and the output value associated with the leaf is returned as the tree’s prediction or forecast. For RF regression, tree uniqueness is ensured by building a select number of trees of identical depth using randomly selected subsamples of the training dataset. To avoid overfitting the data, tree growth is halted when a leaf node has a particular number of values (samples), and the average prediction at that leaf is obtained. To produce a single prediction and to further avoid overfitted data, all trees are averaged together.

A number of parameters can be tuned in an RF model. In this study, the optimal selection of parameters was determined through an iterative method in which the following parameters were methodically varied and the best combination of estimators was chosen: the number of trees, the depth of trees, and the minimum number of

TABLE 1. Nonlinear regression radar retrieval equations derived in this study for D_0 and LWC. Coefficients of the equations are presented with the corresponding bounds on the values.

Retrieval equation	Coef
$D_0 = aZ_H^b Z_{DR}^c$	$a = 0.546 \pm 0.005$
	$b = 0.254 \pm 0.003$
	$c = 0.189 \pm 0.001$
$LWC = aZ_H^b Z_{DR}^c$	$a = 1.48 \times 10^{-6} \pm 5.01 \times 10^{-8}$
	$b = 3.479 \pm 9.37 \times 10^{-3}$
	$c = -0.137 \pm 8.72 \times 10^{-4}$
$RR = aZ_H^b Z_{DR}^c$	$a = 1.377 \times 10^{-6} \pm 4.39 \times 10^{-8}$
	$b = 4.296 \pm 8.75 \times 10^{-3}$
	$c = -0.172 \pm 7.92 \times 10^{-4}$

samples at a leaf. An exhaustive and detailed explanation of RFs, RF regression, and the parameters needed to grow an RF can be found in Breiman (2001). Table 2 documents the optimal parameters chosen in this study’s RF regression. Furthermore, because an RF model cannot be represented by a single equation (as can NL models), this study’s RF model is available online in the form of files containing a Python implementation (<https://github.com/rconrick/NPOL-RF-Retrievals>) for reproduction of results. The RF regressions developed for DSD retrievals, like the NLs above, use Z and Z_{DR} calculated from PARSIVEL² data as input to predict values of D_0 , LWC, and RR.

For consistency, both the NL and RF retrieval methods were developed using the same set of training data. The training data consisted of 50% of the available data, which were randomly selected without replacement. Testing data were the remaining 50%.

c. Computation of N_w

In addition to D_0 and LWC, the normalized intercept parameter is another useful quantity describing the distribution of hydrometeors. Observed DSDs have been shown to fit a gamma distribution (i.e., Ulbrich 1983; Zhang et al. 2008), although many numerical weather prediction models use exponential distributions to describe hydrometeor species because of their computational simplicity (Zhang et al. 2008). As a result, N_w

TABLE 2. Parameters used to generate random forests to predict D_0 and LWC given Z and Z_{DR} as predictors.

	D_0	LWC	RR
No. of trees	50	800	800
Depth of trees	150	50	50
Max data per tree	$(N_{\text{Training}})^{1/2}$	$(N_{\text{Training}})^{1/2}$	$(N_{\text{Training}})^{1/2}$
Min data required to create new branch	4	5	5
Min data per leaf	1	2	2

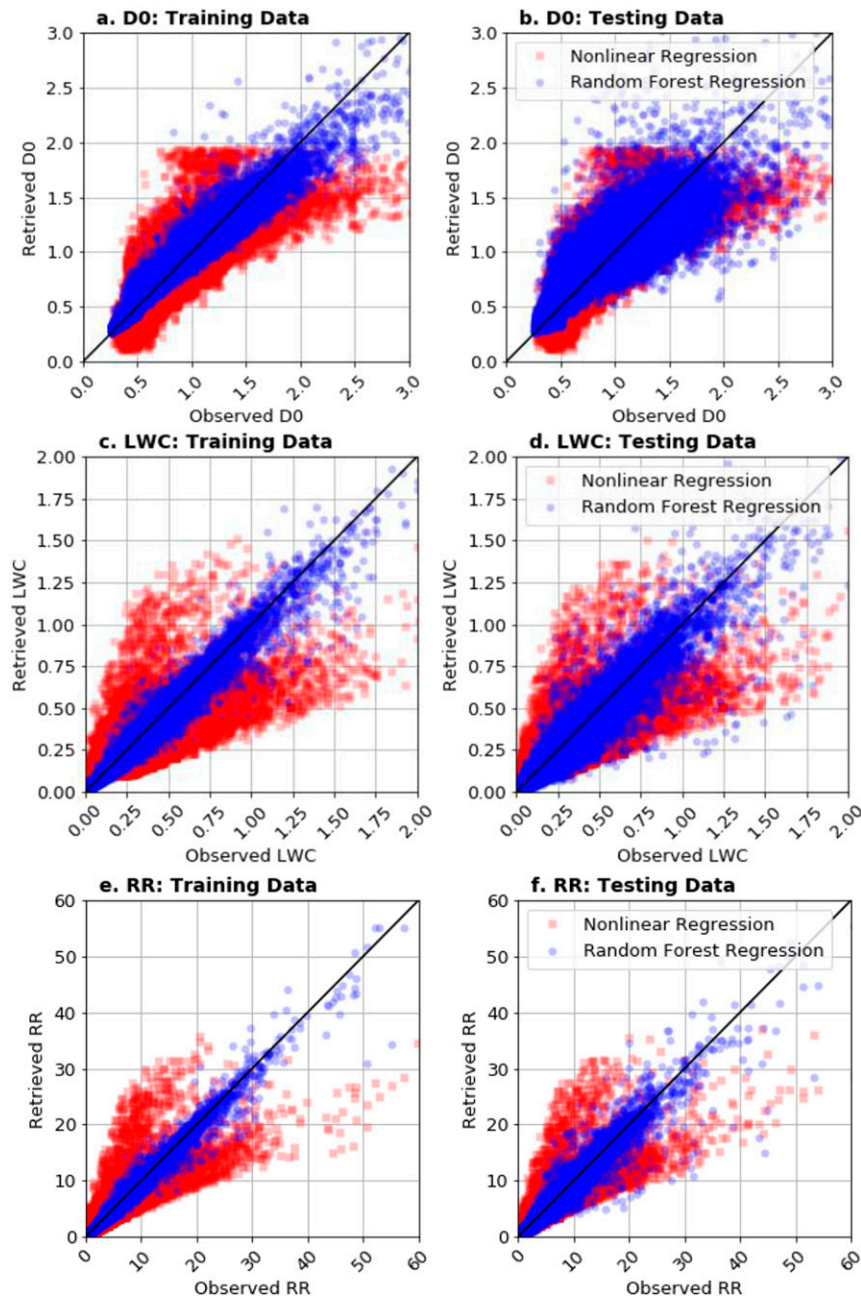


FIG. 3. Scatterplots of PARSIVEL² observed and retrieved (a),(b) D_0 (mm), (c),(d) LWC (g m^{-3}), and (e),(f) RR (mm h^{-1}) from (left) training and (right) testing datasets; each of the training and testing dataset represents a unique 50% of the data selected without replacement. The black line is the 1:1 line. Red squares represent quantities retrieved with nonlinear regression, and the blue circles show quantities obtained by random forest regression.

allows for the direct comparison between observed (gamma) distributions and simulated (exponential) distributions, and it is related to a distribution's raindrop number concentration. From [Thurai et al. \(2014\)](#), N_w is computed by the following relation:

$$N_w = \frac{3.67^4 \times 10^3 \times \text{LWC}}{\pi \rho_w D_0^4},$$

where ρ_w is the density of water (1 g cm^{-3}). To obtain N_w in this study, LWC and D_0 were first obtained from

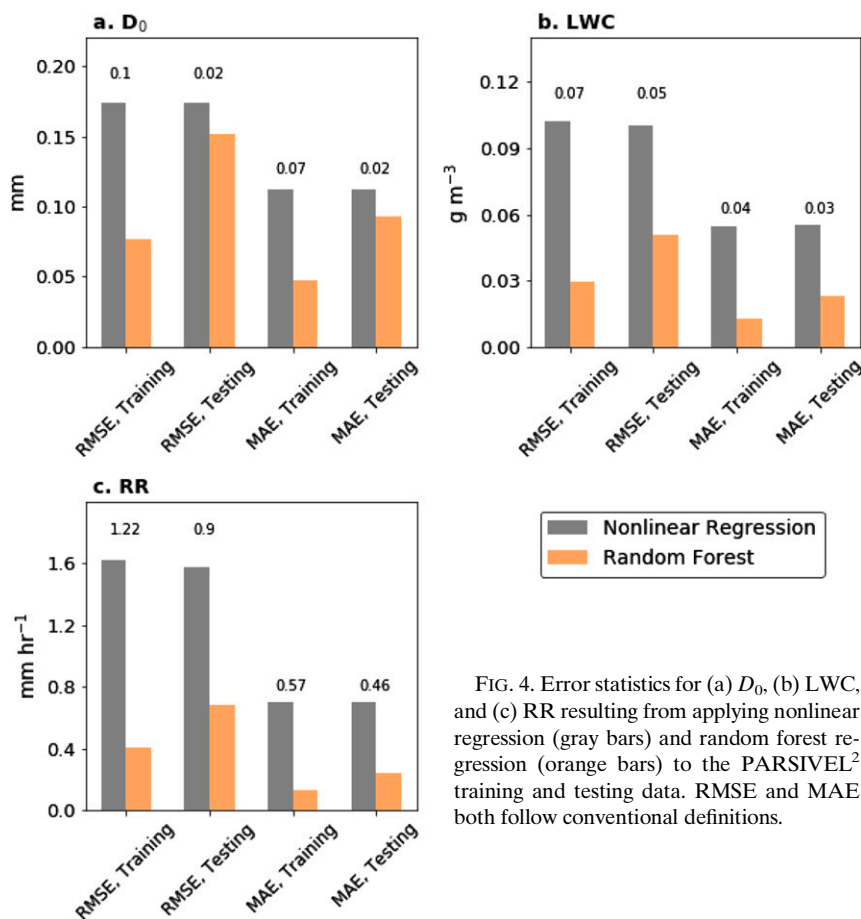


FIG. 4. Error statistics for (a) D_0 , (b) LWC, and (c) RR resulting from applying nonlinear regression (gray bars) and random forest regression (orange bars) to the PARSIVEL² training and testing data. RMSE and MAE both follow conventional definitions.

nonlinear or random forest retrievals and then used as inputs into the above equation. It is important to note that the PARSIVEL² disdrometers also compute N_W this way, but with observed quantities of LWC and D_0 . Thus by following this approach, N_W values are methodologically consistent with surface observing techniques.

4. Evaluation of retrievals

a. Comparison of nonlinear and RF regression

Prior to evaluating retrievals using other observations, retrieval bias was assessed by comparing the NLs and RF method to the PARSIVEL² observations. Figure 3 shows scatterplots of D_0 , LWC, and RR from the training and testing datasets using both retrieval methods. Only PARSIVEL² data were used in Fig. 3 for the purposes of viewing the behavior of the retrievals.

Applying RF retrievals to the testing data shows more retrieved variance for all fields when compared to the training data (Fig. 3), which is expected when considering that the RF is encountering the

testing data for the first time. For small observed D_0 , NL tends to produce erroneously smaller drop sizes than observed, while the RF method does not share this bias (Figs. 3a,b). The RF approach was also better able to capture larger drops, specifically above 2 mm, which appears to be the upper limit for the NL equations. LWC retrievals from the RF method were superior to NLs for all values of LWC, with substantially less spread in the RF retrieval than NLs (Figs. 3c,d). For LWC retrieved from NL, there was overestimation in the training data when values are less than $\sim 0.5\ g\ m^{-3}$ and underestimation above that value. The RR scatterplots in Figs. 3e and 3f demonstrate shapes similar to the LWC plots, but with less variance for both types of retrievals, which is expected considering that RR is a function of LWC.

In all cases, improvement in correlations and a decrease in the differences between observed and retrieved data were found when using RF compared to NL regression. Because we used 1-min DSDs for these comparisons and thus had very large sample sizes, the correlations and slopes were nearly the

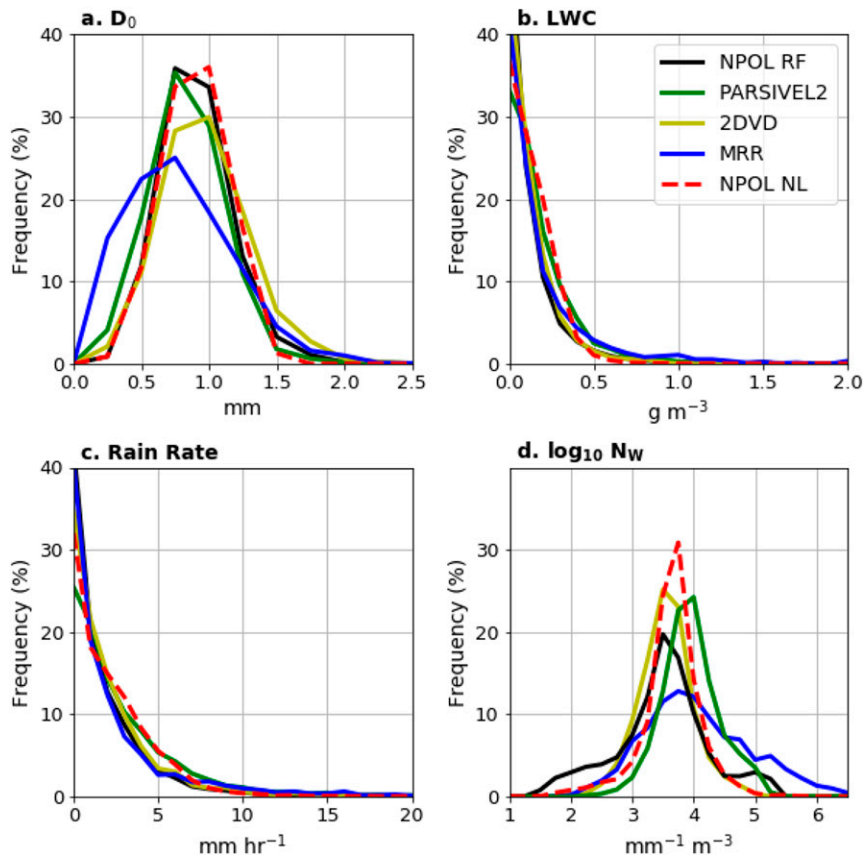


FIG. 5. Frequency distributions of (a) D_0 , (b) LWC, (c) RR, and (d) N_w from surface observations from the PARSIVEL², MRR, and 2DVD networks, NPOL nonlinear regression retrievals (NPOL NL), and NPOL random forest retrievals (NPOL RF). Data are aggregated across all stations for a given network type. See Fig. 1 for the stations that compose each dataset.

same between training and testing data, but improved nonetheless:

- 1) D_0 correlations improved from 0.85 (NL) to 0.93 (random forest) and slopes improved from 0.76 to 0.86,
- 2) LWC correlations improved from 0.74 to 0.97 and slopes improved from 0.53 to 0.94, and
- 3) RR correlations improved from 0.87 to 0.98 and slopes increased from 0.75 to 0.96.

To further highlight the advantages of the RF retrieval method, Fig. 4 shows root-mean-square errors (RMSE) and mean absolute errors (MAE) for the data presented in Fig. 3. For NL retrievals, training and testing data errors are comparable, which is the result of these retrievals applying a fixed functional form to the data. Using RF retrievals, however, had a dramatic impact on error statistics, with many error quantities being reduced by well over 50%. One notable outlier is the RF retrieval applied to D_0 testing data, which improved

less than for the other fields. This can also be noted from comparing Figs. 4a and 4b, which demonstrate broader distributions of D_0 retrievals from training to testing datasets.

b. Independent data evaluation at the surface

To evaluate RF DSD retrievals, observations of DSD parameters were considered from the 2DVDs and the MRRs that were collocated with PARSIVEL² units (Fig. 1). The following evaluations are presented using surface data that are collocated in time and space as described previously. MRR data shown are from the second gate above the surface, at 125 m AGL.

Frequency distributions of D_0 , LWC, N_w , and RR from PARSIVEL², MRR, and 2DVD observations at the surface are shown in Fig. 5 along with the same quantities retrieved from NPOL random forest and NL techniques. Data in Fig. 5 are aggregated by instrument type. Figure 5a shows that D_0 observations from PARSIVEL² and 2DVD were similar, although

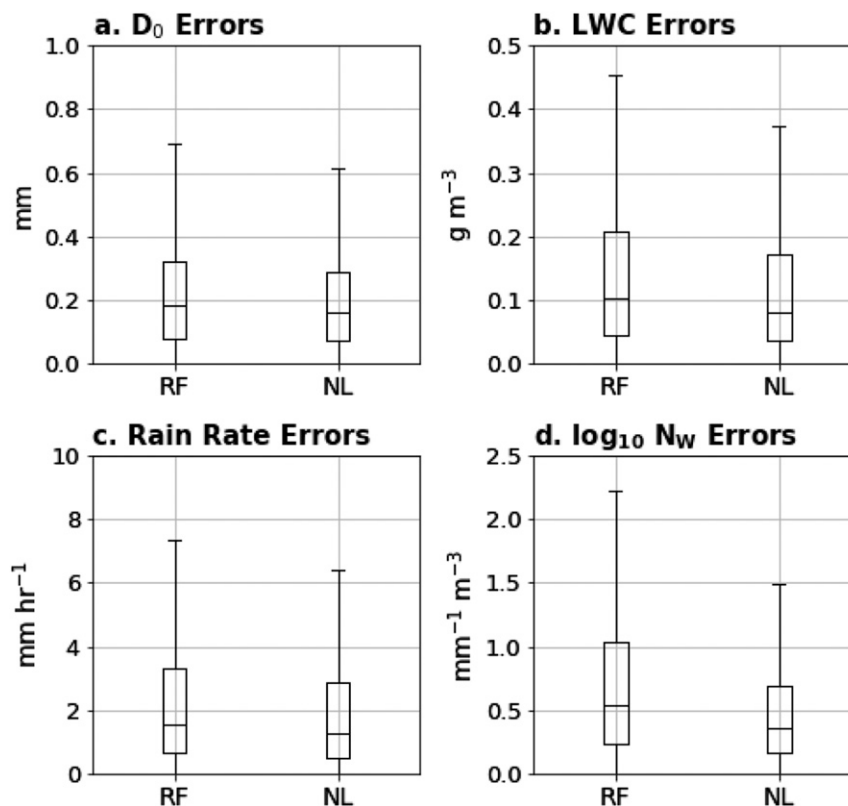


FIG. 6. Boxplots (25, 50, and 75 percentiles, from bottom to top) showing the absolute errors of NPOL random forest (RF) and nonlinear regression (NL) retrievals in comparison with PARSIVEL² disdrometer data aggregated at all PARSIVEL² sites in Fig. 1.

PARSIVEL² observations had a peak frequency at 0.75 mm whereas 2DVD observations peaked slightly larger. In comparing RF with NL retrievals, it is seen that RF captured the smaller peak drop size whereas NL tended toward larger peak sizes. Otherwise, distributions of RF and NL retrieved D_0 was similar. For D_0 observations, the MRR was shifted toward very small values of D_0 , and thus was an outlier. Across observations and retrievals, LWC and RR distributions (Figs. 5b,c, respectively) were all approximately exponential and qualitatively similar in terms of magnitudes. Subtle differences, though, exist between the RF and NL retrieval accuracy. Specifically, RF retrievals tend to favor lower values of LWC and RR, whereas the NL retrievals favor larger values, although neither could be qualitatively considered outliers given the spread of observations. Both methods overpredict very low LWC and RR when compared to PARSIVEL² observations, which is a result of using PARSIVEL² rain rates to filter other datasets. Finally, Fig. 5d shows N_w calculated from D_0 and LWC as described previously. Because N_w is a function of D_0^{-4} , the errors in Fig. 5a are magnified. Interestingly, the RF

retrieval produces N_w values that are closer to the 2DVD observations than the PARSIVEL². The RF retrieval also produces a number of very small N_w values that are not well captured by the other platforms, although they may also be a result of no rain noted by the radar despite the PARSIVEL² recording precipitation. As in Fig. 5a, N_w data from the MRRs are outliers at the surface, where the distribution in Fig. 5c is much broader than the other platforms and favors very large N_w . Figure 6 presents distributions of absolute error between PARSIVEL² observations and the RF or NL retrievals. None of the error distributions for a particular retrieved quantity are statistically different as per a Kolmogorov–Smirnov similarity test. This can be inferred visually from the considerable overlap in the errors between retrieval techniques. Despite these results, RF retrievals do offer considerable advantages. In particular, as shown in Fig. 3, because RF retrievals are not confined to fixed functional form, they have more flexibility to retrieve a broader range of values. It is suspected that the minimal differences between RF and NL errors in Fig. 6 are chiefly the result of NPOL beam height

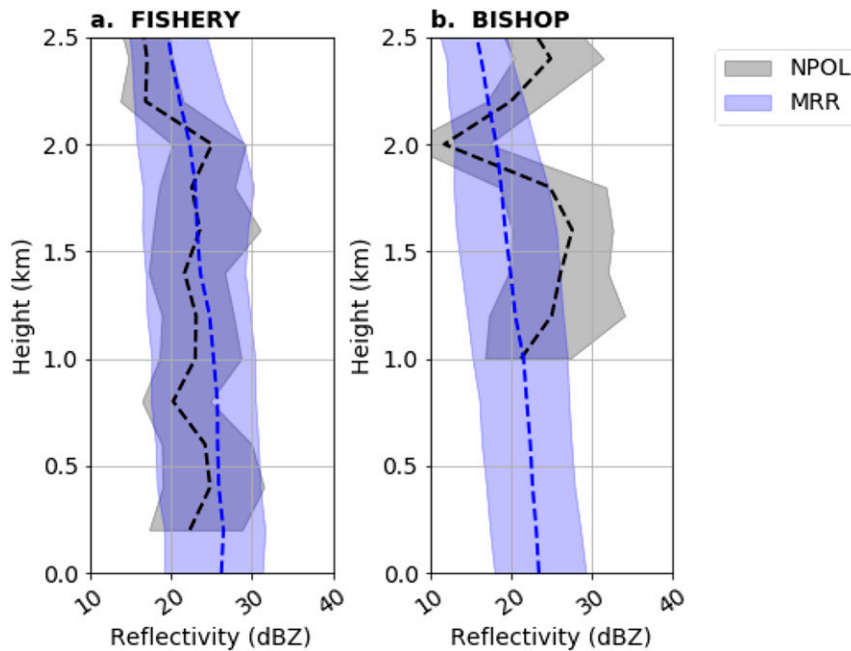


FIG. 7. Vertical profiles of radar reflectivity at the (a) Fishery site and (b) Bishop Field from the NPOL radar (black) and MRRs (blue). Shaded regions indicate the interquartile range, and the dashed lines show the median value; 1-min MRR data are used at the observation times of the NPOL radar along the 49.9° RHI scan.

above the surface stations, which introduces error into the retrievals.

c. Qualitative comparisons with MRR data

As a final evaluation, NPOL retrievals are compared to MRR profiles from the surface to 2.5 km AGL. For this study, the MRRs located at the Fishery and Bishop Field sites were used. It is important to note that because of data quality concerns (J. Zagrodnik 2019, personal communication) the MRRs have not been used extensively in OLYMPLEX literature. Nonetheless, it is important to compare them qualitatively to the NPOL retrievals. Figure 7 shows vertical profiles of the interquartile range and median reflectivity from the MRRs and NPOL radar. At the Fishery site, agreement between platforms is considered good, with only minor deviations between radar profiles (Fig. 7a). At Bishop Field, however, the discrepancies between NPOL and MRR data are more substantial and thus Bishop Field data were excluded from profile analyses in Fig. 8. Data for the vertical profiles in Figs. 7 and 8 are binned every 200 m altitude.

Vertical profiles of D_0 , LWC, RR, and N_W are presented in Fig. 8 from NPOL RF retrievals and MRR at the Fishery site. For all fields, accuracy decreases significantly above 1 km AGL, with the best agreement noted below 0.5 km AGL. Furthermore, some overlap is noted in data interquartile ranges from 1 to 1.5 km. As in

the surface analyses presented above, the NPOL RF and NL retrievals perform similarly, with a notable exception being the D_0 retrievals, for which NPOL RF produces smaller and more reasonable D_0 . The smaller drops from RF D_0 are more physically reasonable given that warm rain processes are favored in the environment of the Olympic Peninsula (Zagrodnik et al. 2018). Because reflectivity from the MRR is calculated using the measured DSD, it is possible that the similar reflectivity profiles at Fishery in Fig. 7a are the result of MRR DSD errors increasing as a function of height. For instance, the strong decrease in MRR D_0 as a function of height is contrary to other studies using MRR instruments, which found a less pronounced decrease or nearly constant profile (Chen et al. 2016; Marzuki et al. 2016), with the smaller drop sizes seen by the MRR at the surface in Fig. 6a lending credibility to possible MRR errors. Although there are potential MRR data problems aloft, they are included in this study to highlight the need for better observations of DSDs below the melting level. Nonetheless, agreement between NPOL retrievals and the MRR data near the surface in Fig. 8 does indicate that NPOL retrievals are skillful near the surface.

5. Discussion and concluding remarks

In this study, nonlinear and random forest regressions are used to develop dual-polarization radar retrievals

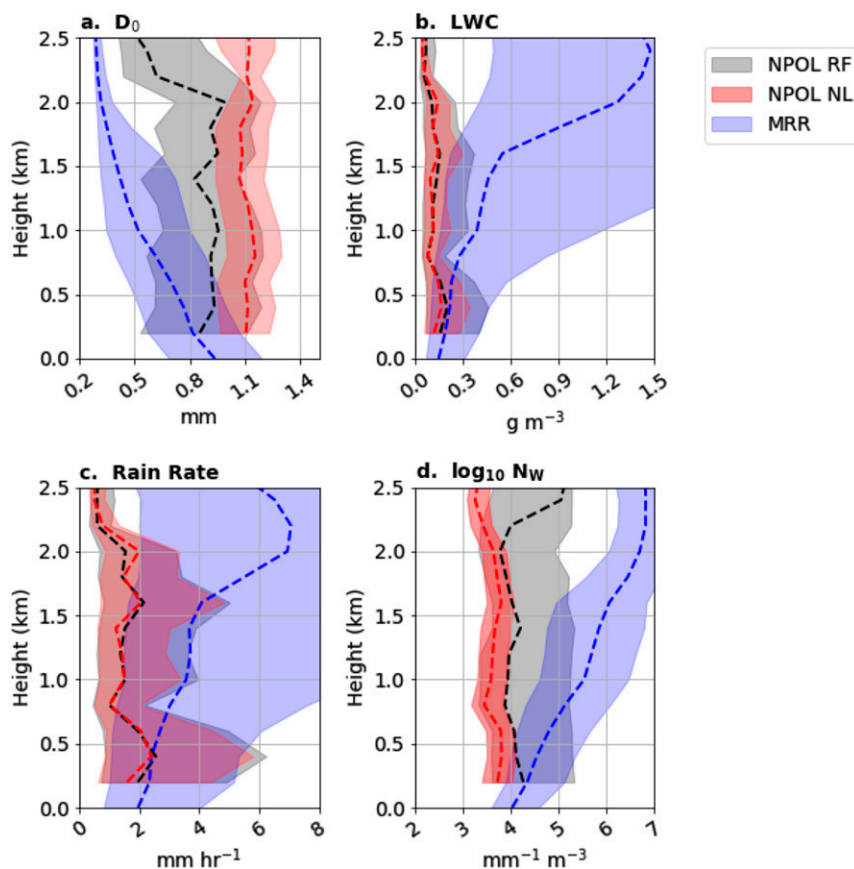


FIG. 8. Vertical profiles of (a) D_0 , (b) LWC, (c) RR, and (d) N_w at the Fishery site from the NPOL RF retrievals (black), NPOL NL retrievals (red), and MRRs (blue). Shaded regions indicate the interquartile range, and the dashed lines show the median value; 1-min MRR data are used at the observation times of the NPOL radar along the 49.9° RHI scan.

using NPOL radar observations from the OLYMPEX field experiment of 2015/16. Radar retrievals were developed for the median volume diameter D_0 , liquid water content, and rain rate using observations from six PARSIVEL² disdrometers, with the normalized drop size distribution intercept parameter N_w computed as a function of LWC and D_0 . After development, initial evaluations showed that the random forest retrievals in this study were more accurate and unbiased than non-linear regression retrievals when applied to and evaluated against the PARSIVEL² disdrometer dataset, with some improvements in RMSE exceeding 50%. Correlations and slopes describing the relationship between observed and retrieved values increased for all quantities when RF methods were used, with the most substantial increase being LWC having a slope increase from 0.53 to 0.94.

Two independent datasets, 2DVDs and MRR vertically pointing radars were used to evaluate retrievals at the surface using 1-min data from the OLYMPEX winter matched to NPOL observation times. Results demonstrated a high degree of correspondence between

PARSIVEL², 2DVD, and MRR observations, except for MRR D_0 and N_w . Differences between RF and NL retrievals were also shown to be modest based on analysis of mean errors relative to PARSIVEL² data, although the utility of RF retrievals is evident for more extreme values. Above the surface, where very little microphysical information is available, the MRRs were used to qualitatively assess NPOL retrievals at the Fishery site. Below 500 m AGL, there was good agreement between NPOL and MRR data, with lesser but still reasonable agreement for 0.5–1 km AGL. The RF D_0 retrievals were more accurate than the NL retrieval at low levels.

Although the results of RF retrievals are not significantly better than NL retrievals when applied to the entire OLYMPEX winter, RF retrievals were shown to offer some key advantages. Figure 3 demonstrated the disadvantage of using a fixed functional form to retrieve DSDs, as in an NL retrieval. Using an NL approach introduces a greater number of erroneous data points, as is evident, for instance, by the ~ 2 -mm cutoff for

NL D_0 retrievals in Figs. 3a and 3b that is not seen in the RF retrievals. Thus, while overall error statistics from RF retrievals may not be appreciably different than NL retrievals, the method employed to produce RF retrievals is more conducive to obtaining DSDs that are physically accurate and less prone to spurious large errors.

Furthermore, despite developing retrievals over a particular region, it is likely that this approach is more widely applicable, as liquid precipitation regimes consisting of numerous small drops have been noted in cloud systems around the world (e.g., Thompson et al. 2015; Dolan et al. 2018). Furthermore, the application of random forest regression to radar retrieval provides a novel retrieval method that is at least as accurate as traditional nonlinear regression to obtain DSD characteristics from dual-polarimetric data, with the potential to better capture D_0 .

The development and evaluation of above-surface retrievals is important for advancing understanding of precipitation characteristics, particularly when combined with other observing methods. Because previous evaluations of precipitation simulations in over the windward side of the Olympic Mountains have found precipitation underprediction, future research will employ this new approach to better understand numerical weather prediction model biases in the context of simulated and observed DSDs.

Acknowledgments. This work was supported by the National Science Foundation through Grant AGS-1349847. The authors acknowledge Joseph Hardin for his advice on radar retrievals, and three anonymous reviewers whose suggestions greatly improved the manuscript.

REFERENCES

- Adirosi, E., L. Baldini, N. Roberto, P. Gatlin, and A. Tokay, 2016: Improvement of vertical profiles of raindrop size distribution from Micro Rain Radar using 2D video disdrometer measurements. *Atmos. Res.*, **169**, 404–415, <https://doi.org/10.1016/j.atmosres.2015.07.002>.
- Apffel, K. R., A. Reynolds, and D. Zaff, 2015: Improving the quantitative precipitation estimate for hydrometeors classified as dry snow by polarimetric radars. NOAA/National Weather Service Eastern Regional Tech. Attachment 2015-06, 10 pp., <https://www.weather.gov/media/erh/ta2015-06.pdf>.
- Atlas, D., R. C. Srivastava, and R. S. Sekhon, 1973: Doppler radar characteristics of precipitation at vertical incidence. *Rev. Geophys.*, **11**, 1–35, <https://doi.org/10.1029/RG011i001p00001>.
- , C. W. Ulbrich, F. D. Marks Jr., E. Amitai, and C. R. Williams, 1999: Systematic variation of drop size and radar-rainfall relations. *J. Geophys. Res.*, **104**, 6155–6169, <https://doi.org/10.1029/1998JD200098>.
- Baldini, L., V. Chandrasekar, and D. Moisseev, 2012: Microwave radar signatures of precipitation from S band to Ka band: Application to GPM mission. *Eur. J. Remote Sens.*, **45**, 75–88, <https://doi.org/10.5721/EuJRS20124508>.
- Beard, K. V., 1976: Terminal velocity and shape of cloud and precipitation drops aloft. *J. Atmos. Sci.*, **33**, 851–864, [https://doi.org/10.1175/1520-0469\(1976\)033<0851:TVASOC>2.0.CO;2](https://doi.org/10.1175/1520-0469(1976)033<0851:TVASOC>2.0.CO;2).
- Brandes, E. A., G. Zhang, and J. Vivekanandan, 2004a: Comparison of polarimetric radar drop size distribution retrieval algorithms. *J. Atmos. Oceanic Technol.*, **21**, 584–598, [https://doi.org/10.1175/1520-0426\(2004\)021<0584:COPRDS>2.0.CO;2](https://doi.org/10.1175/1520-0426(2004)021<0584:COPRDS>2.0.CO;2).
- , —, and —, 2004b: Drop size distribution retrieval with polarimetric radar: Model and application. *J. Appl. Meteor.*, **43**, 461–475, [https://doi.org/10.1175/1520-0450\(2004\)043<0461:DSDRWP>2.0.CO;2](https://doi.org/10.1175/1520-0450(2004)043<0461:DSDRWP>2.0.CO;2).
- , —, and J. Sun, 2006: On the influence of assumed drop size distribution form on radar-retrieved thunderstorm microphysics. *J. Appl. Meteor. Climatol.*, **45**, 259–268, <https://doi.org/10.1175/JAM2335.1>.
- Breiman, L., 2001: Random forests. *Mach. Learn.*, **45**, 5–32, <https://doi.org/10.1023/A:1010933404324>.
- Bringi, V. N., V. Chandrasekar, N. Balakrishnan, and D. S. Zrnić, 1990: An examination of propagation effects in rainfall on radar measurements at microwave frequencies. *J. Atmos. Oceanic Technol.*, **7**, 829–840, [https://doi.org/10.1175/1520-0426\(1990\)007<0829:AEOPEI>2.0.CO;2](https://doi.org/10.1175/1520-0426(1990)007<0829:AEOPEI>2.0.CO;2).
- , —, J. Hubbert, E. Gorgucci, W. L. Randeu, and M. Schoenhuber, 2003: Raindrop size distribution in different climatic regimes from disdrometer and dual-polarized radar analysis. *J. Atmos. Sci.*, **60**, 354–365, [https://doi.org/10.1175/1520-0469\(2003\)060<0354:RSDIDC>2.0.CO;2](https://doi.org/10.1175/1520-0469(2003)060<0354:RSDIDC>2.0.CO;2).
- , C. R. Williams, M. Thurai, and P. T. May, 2009: Using dual-polarized radar and dual-frequency profiler for DSD characterization: A case study from Darwin, Australia. *J. Atmos. Oceanic Technol.*, **26**, 2107–2122, <https://doi.org/10.1175/2009JTECHA1258.1>.
- , G. Huang, S. J. Munchak, C. D. Kummerow, D. A. Marks, and D. B. Wolff, 2012: Comparison of drop size distribution parameter (D_0) and rain rate from S-band dual-polarized ground radar, TRMM Precipitation Radar (PR), and Combined PR–TMI: Two events from Kwajalein Atoll. *J. Atmos. Oceanic Technol.*, **29**, 1603–1616, <https://doi.org/10.1175/JTECH-D-11-00153.1>.
- Cao, Q., G. Zhang, E. Brandes, T. Schuur, A. Ryzhkov, and K. Ikeda, 2008: Analysis of video disdrometer and polarimetric radar data to characterize rain microphysics in Oklahoma. *J. Appl. Meteor. Climatol.*, **47**, 2238–2255, <https://doi.org/10.1175/2008JAMC1732.1>.
- Carlin, J. T., A. V. Ryzhkov, J. C. Snyder, and A. Khain, 2016: Hydrometeor mixing ratio retrievals for storm-scale radar data assimilation: Utility of current relations and potential benefits of polarimetry. *Mon. Wea. Rev.*, **144**, 2981–3001, <https://doi.org/10.1175/MWR-D-15-0423.1>.
- Chandrasekar, V., A. Hou, E. Smith, V. N. Bringi, S. A. Rutledge, E. Gorgucci, W. A. Petersen, and G. S. Jackson, 2008: Potential role of dual-polarization radar in the validation of satellite precipitation measurements. *Bull. Amer. Meteor. Soc.*, **89**, 1127–1146, <https://doi.org/10.1175/2008BAMS2177.1>.
- Chen, Y., J. An, H. Liu, and J. Duan, 2016: An observational study on vertical raindrop size distributions during stratiform rain in a semiarid plateau climate zone. *Atmos. Ocean. Sci. Lett.*, **9**, 178–184, <https://doi.org/10.1080/16742834.2016.1169151>.
- Chow, F. K., B. J. Snyder, and S. F. J. de Wekker, 2013: *Mountain Weather Research and Forecasting: Recent Progress and Current Challenges*. Springer, 750 pp.

- Conrick, R., and C. F. Mass, 2019a: Evaluating simulated microphysics during OLYMPEX using GPM satellite observations. *J. Atmos. Sci.*, **76**, 1093–1105, <https://doi.org/10.1175/JAS-D-18-0271.1>.
- , and —, 2019b: An evaluation of simulated precipitation characteristics during OLYMPEX. *J. Hydrometeorol.*, **20**, 1147–1164, <https://doi.org/10.1175/JHM-D-18-0144.1>.
- Dolan, B., B. Fuchs, S. A. Rutledge, E. A. Barnes, and E. J. Thompson, 2018: Primary modes of global drop size distributions. *J. Atmos. Sci.*, **75**, 1453–1476, <https://doi.org/10.1175/JAS-D-17-0242.1>.
- Fulton, R., 2002: Improving NWS WSR-88D rainfall algorithms and products at the Hydrology Laboratory. *NEXRAD Technical Advisory Committee Meeting*, Norman, OK, NOAA, https://www.nws.noaa.gov/ohd/hrl/papers/wsr88d/tac_nov02.pdf.
- Gorgucci, E., V. Chandrasekar, and L. Baldini, 2008: Microphysical retrievals from dual-polarization radar measurements at X band. *J. Atmos. Oceanic Technol.*, **25**, 729–741, <https://doi.org/10.1175/2007JTECHA971.1>.
- Gu, J., A. Ryzhkov, P. Zhang, P. Neilley, M. Knight, B. Wolf, and D. Lee, 2011: Polarimetric attenuation correction in heavy rain at C band. *J. Appl. Meteor. Climatol.*, **50**, 39–58, <https://doi.org/10.1175/2010JAMC2258.1>.
- Hardin, J., and N. Guy, 2017: PyDisdrometer: Python library for working with disdrometer data. Zenodo, <https://doi.org/10.5281/zenodo.9991>.
- Helmus, J. J., and S. M. Collis, 2016: The Python ARM Radar Toolkit (Py-ART), a library for working with weather radar data in the Python programming language. *J. Open Res. Software*, **4**, e25, <https://doi.org/10.5334/jors.119>.
- Herman, G. R., and R. S. Schumacher, 2018: Money doesn't grow on trees, but forecasts do: Forecasting extreme precipitation with random forests. *Mon. Wea. Rev.*, **146**, 1571–1600, <https://doi.org/10.1175/MWR-D-17-0250.1>.
- Hou, A. Y., and Coauthors, 2014: The Global Precipitation Measurement Mission. *Bull. Amer. Meteor. Soc.*, **95**, 701–722, <https://doi.org/10.1175/BAMS-D-13-00164.1>.
- Houze, R. A., Jr., and Coauthors, 2017: The Olympic Mountains Experiment (OLYMPEX). *Bull. Amer. Meteor. Soc.*, **98**, 2167–2188, <https://doi.org/10.1175/BAMS-D-16-0182.1>.
- Illingworth, A. J., and T. M. Blackman, 2002: The need to represent raindrop size spectra as normalized gamma distributions for the interpretation of polarization radar observations. *J. Appl. Meteor.*, **41**, 286–297, [https://doi.org/10.1175/1520-0450\(2002\)041<0286:TNTRRS>2.0.CO;2](https://doi.org/10.1175/1520-0450(2002)041<0286:TNTRRS>2.0.CO;2).
- Jensen, M. P., and Coauthors, 2016: The Midlatitude Continental Convective Clouds Experiment (MC3E). *Bull. Amer. Meteor. Soc.*, **97**, 1667–1686, <https://doi.org/10.1175/BAMS-D-14-00228.1>.
- Krajewski, W., B. C. Seo, R. Goska, I. Demir, and M. Elsaadani, 2013: Precipitation datasets for the GPM Iowa Flood Studies (IFloodS) field experiment. *Geophysical Research Abstracts*, Vol. 15, Abstract EGU2013-11303, <http://meetingorganizer.copernicus.org/EGU2013/EGU2013-11303.pdf>.
- Kuligowski, R. J., 1997: An overview of National Weather Service quantitative precipitation estimates. National Weather Service Techniques Development Laboratory Office Note 97-4, 28 pp., <https://www.nws.noaa.gov/im/pub/tdl97-4.pdf>.
- Kumjian, M. R., 2013: Principles and applications of dual-polarization weather radar. Part I: Description of the polarimetric radar variables. *J. Oper. Meteor.*, **1**, 226–242, <https://doi.org/10.15191/nwajom.2013.0119>.
- Marshall, J. S., and W. McK. Palmer, 1948: The distribution of raindrops with size. *J. Meteor.*, **5**, 165–166, [https://doi.org/10.1175/1520-0469\(1948\)005<0165:TDORWS>2.0.CO;2](https://doi.org/10.1175/1520-0469(1948)005<0165:TDORWS>2.0.CO;2).
- Marzuki, M., H. Hashiguchi, T. Shimomai, I. Rahayu, and M. Vonnisa, 2016: Performance evaluation of Micro Rain Radar over Sumatra through comparison with disdrometer and wind profiler. *Prog. Electromagn. Res.*, **50**, 33–46, <https://doi.org/10.2528/PIERM16072808>.
- METEK, 2009: MRR physical basics: Version 5.2.0.1. METEK Rep., 20 pp., http://www.mpimet.mpg.de/fileadmin/atmosferaere/barbados/Instrumentation/MRR-physical-basics_20090707.pdf.
- Mishchenko, M. I., L. D. Travis, and D. W. Mackowski, 1996: T-matrix computations of light scattering by nonspherical particles: A review. *J. Quant. Spectrosc. Radiat. Transfer*, **55**, 535–575, [https://doi.org/10.1016/0022-4073\(96\)00002-7](https://doi.org/10.1016/0022-4073(96)00002-7).
- Pedregosa, F., and Coauthors, 2011: Scikit-learn: Machine learning in Python. *J. Mach. Learn. Res.*, **12**, 2825–2830, <http://www.jmlr.org/papers/volume12/pedregosa11a/pedregosa11a.pdf>.
- Peters, G., B. Fischer, H. Münster, M. Clemens, and A. Wagner, 2005: Profiles of raindrop size distributions as retrieved by microrain radars. *J. Appl. Meteor.*, **44**, 1930–1949, <https://doi.org/10.1175/JAM2316.1>.
- Petersen, W. A., and P. N. Gatlin, 2017: GPM Ground Validation Micro Rain Radar (MRR) OLYMPEX. NASA Global Hydrology Resource Center DAAC. Subset used: Bishop Field and Fishery, accessed 1 February 2019, <https://doi.org/10.5067/GPMGV/OLYMPEX/MRR/DATA201>.
- , A. Tokay, P. N. Gatlin, and M. T. Wingo, 2017a: GPM Ground Validation Autonomous Parsivel Unit (APU) OLYMPEX. NASA Global Hydrology Resource Center DAAC. Subset used: APU01, APU02, APU03, APU05, APU06, APU08, APU09, and APU11, November–December 2015, accessed 1 February 2019, <https://doi.org/10.5067/GPMGV/OLYMPEX/APU/DATA301>.
- , D. Wolff, M. T. Wingo, and A. Tokay, 2017b: GPM Ground Validation two-dimensional video disdrometer (2DVD) OLYMPEX. NASA Global Hydrology Resource Center DAAC. Subset used: Amanda Park, Bishop Field, and Fishery, accessed 1 February 2019, <https://doi.org/10.5067/GPMGV/OLYMPEX/2DVD/DATA/301>.
- Pippitt, J. L., D. A. Marks, and D. B. Wolff, 2013: Dual polarimetric quality control for NASA's Global Precipitation Measurement (GPM) Mission Ground Validation program. *36th Conf. on Radar Meteorology*, Breckenridge, CO, Amer. Meteor. Soc., <https://ams.confex.com/ams/36Radar/webprogram/Manuscript/Poster228522/DPOCManuscript.pdf>.
- , D. B. Wolff, W. A. Petersen, and D. A. Marks, 2015: Data and operational processing for NASA's GPM Ground Validation program. *37th Conf. on Radar Meteorology*, Norman, OK, Amer. Meteor. Soc., 111, <https://ams.confex.com/ams/37RADAR/webprogram/Paper275627.html>.
- Ryzhkov, A., M. Diederich, P. Zhang, and C. Simmer, 2014: Potential utilization of specific attenuation for rainfall estimation, mitigation of partial beam blockage, and radar networking. *J. Atmos. Oceanic Technol.*, **31**, 599–619, <https://doi.org/10.1175/JTECH-D-13-00038.1>.
- Seifert, A., 2005: On the shape–slope relation of drop size distributions in convective rain. *J. Appl. Meteor.*, **44**, 1146–1151, <https://doi.org/10.1175/JAM2254.1>.
- Sharma, S., M. Konwar, D. K. Sarma, M. C. Kalapureddy, and A. R. Jain, 2009: Characteristics of rain integral parameters during tropical convective, transition, and stratiform rain at Gadanki and its application in rain retrieval. *J. Appl. Meteor. Climatol.*, **48**, 1245–1266, <https://doi.org/10.1175/2008JAMC1948.1>.
- Thompson, E. J., S. A. Rutledge, B. Dolan, and M. Thurai, 2015: Drop size distributions and radar observations of convective and stratiform rain over the equatorial Indian and west Pacific

- Oceans. *J. Atmos. Sci.*, **72**, 4091–4125, <https://doi.org/10.1175/JAS-D-14-0206.1>.
- Thurai, M., and V. N. Bringi, 2005: Drop axis ratios from a 2D video disdrometer. *J. Atmos. Oceanic Technol.*, **22**, 966–978, <https://doi.org/10.1175/JTECH1767.1>.
- , —, and P. T. May, 2010: CPOL radar-derived drop size distribution statistics of stratiform and convective rain for two regimes in Darwin, Australia. *J. Atmos. Oceanic Technol.*, **27**, 932–942, <https://doi.org/10.1175/2010JTECHA1349.1>.
- , C. R. Williams, and V. N. Bringi, 2014: Examining the correlations between drop size distribution parameters using data from two side-by-side 2D-video disdrometers. *Atmos. Res.*, **144**, 95–110, <https://doi.org/10.1016/j.atmosres.2014.01.002>.
- Tokay, A., and D. A. Short, 1996: Evidence from tropical raindrop spectra of the origin of rain from stratiform versus convective clouds. *J. Appl. Meteor.*, **35**, 355–371, [https://doi.org/10.1175/1520-0450\(1996\)035<0355:EFTRSO>2.0.CO;2](https://doi.org/10.1175/1520-0450(1996)035<0355:EFTRSO>2.0.CO;2).
- , A. Kruger, and W. F. Krajewski, 2001: Comparison of drop size distribution measurements by impact and optical disdrometers. *J. Appl. Meteor.*, **40**, 2083–2097, [https://doi.org/10.1175/1520-0450\(2001\)040<2083:CODSDM>2.0.CO;2](https://doi.org/10.1175/1520-0450(2001)040<2083:CODSDM>2.0.CO;2).
- , D. B. Wolff, and W. A. Petersen, 2014: Evaluation of the new version of the laser-optical disdrometer, OTT Parsivel². *J. Atmos. Oceanic Technol.*, **31**, 1276–1288, <https://doi.org/10.1175/JTECH-D-13-00174.1>.
- Uijlenhoet, R., M. Steiner, and J. A. Smith, 2003: Variability of raindrop size distributions in a squall line and implications for radar rainfall estimation. *J. Hydrometeor.*, **4**, 43–61, [https://doi.org/10.1175/1525-7541\(2003\)004<0043:VORSDDI>2.0.CO;2](https://doi.org/10.1175/1525-7541(2003)004<0043:VORSDDI>2.0.CO;2).
- Ulbrich, C. W., 1983: Natural variations in the analytical form of the raindrop size distribution. *J. Climate Appl. Meteor.*, **22**, 1764–1775, [https://doi.org/10.1175/1520-0450\(1983\)022<1764:NVITAF>2.0.CO;2](https://doi.org/10.1175/1520-0450(1983)022<1764:NVITAF>2.0.CO;2).
- Wolff, D., D. A. Marks, W. A. Petersen, and J. Pippit, 2017: GPM Ground Validation NASA S-band dual polarimetric (NPOL) Doppler radar OLYMPEX. NASA Global Hydrology Resource Center DAAC, accessed 1 February 2019, <https://doi.org/10.5067/GPMGV/OLYMPEX/NPOL/DATA301>.
- Zagrodnik, J. P., L. A. McMurdie, and R. A. Houze Jr., 2018: Stratiform precipitation processes in cyclones passing over a coastal mountain range. *J. Atmos. Sci.*, **75**, 983–1004, <https://doi.org/10.1175/JAS-D-17-0168.1>.
- Zhang, G., J. Vivekanandan, and E. Brandes, 2001: A method for estimating rain rate and drop size distribution from polarimetric radar measurements. *IEEE Trans. Geosci. Remote Sens.*, **39**, 830–841, <https://doi.org/10.1109/36.917906>.
- , J. Sun, and E. A. Brandes, 2006: Improving parameterization of rain microphysics with disdrometer and radar observations. *J. Atmos. Sci.*, **63**, 1273–1290, <https://doi.org/10.1175/JAS3680.1>.
- , M. Xue, Q. Cao, and D. Dawson, 2008: Diagnosing the intercept parameter for exponential raindrop size distribution based on video disdrometer observations: Model development. *J. Appl. Meteor. Climatol.*, **47**, 2983–2992, <https://doi.org/10.1175/2008JAMC1876.1>.